國立雲林科技大學
97學年度博士班招生考試試題

所別：化學工程與材料工程系
科目：科技文獻

一、 請針對附件一內容，回答下列問題

1. 本篇論文研究目的為何? (10%)

2. 本篇論文實驗步驟為何? (10%)

3. 本篇論文如何驗證其實驗結果? (15%)

4. 本篇論文有何發現及具體成果? (15%)

二、 請針對附件二內容，回答下列問題

1. 本篇論文中有提及那些提高 CNT 之比電容(specific capacitance)的方法? 而本篇論文所採取提高 MWCNT 之比電容的方法與其學理為何？ (35%)

2. 本篇論文的重要結論與具體貢獻為何？ (15%)

國立雲林科技大學
97學年度博士班招生考試試題

所別：化學工程與材料工程系
科目：科技文獻

附件一

Self-Cleaning Particle Coating with Antireflection Properties

Xin-Tong Zhang,† Osamu Sato,† Minori Taguchi,‡ Yasuaki Einaga,‡ Taketoshi Murakami,† and Akira Fujishima*,†

Special Laboratory for Optical Sciences, Kanagawa Academy of Science and Technology, 3-2-1 Sakado, Takatsu-ku, Kawasaki-shi, Kanagawa 213-0012, Japan, and Department of Chemistry, Faculty of Science and Technology, Keio University, 3-14-1 Hiyoshi, Kanagawa 223-8522, Japan

Received September 14, 2004. Revised Manuscript Received November 16, 2004

We report here a self-cleaning particle coating with antireflection (AR) properties. The coatings were prepared by (1) depositing SiO_2 single-layered particle coatings on polyelectrolyte-modified glass substrates through electrostatic attraction, (2) subsequently depositing another layer of TiO_2 nanoparticles through electrostatic attraction, and (3) removing the polymer by calcination at 500 °C. The AR effect of the coatings was studied with transmission spectra collected at normal incidence. The self-cleaning properties of the coatings were studied by the change of the water contact angle on octadodecyldimethylchlorosilane-modified coatings under 1.0 mW cm^{-2} ultraviolet light. Both the AR and self-cleaning properties of the coatings were dependent on the concentration of colloidal TiO_2 solution used in the preparation. However, excellent surface wettability of the coatings for water was obtained, independent of the preparation conditions. The experimental findings are discussed in terms of the special structure of the particle coatings.

Introduction

A coating with self-cleaning properties would be interesting and attractive since it could save a lot of time and cost for maintenance.[1] A natural self-cleaning surface, the lotus leaf, stays clean by means of rainwater droplets, which roll off the superhydrophobic leaf surface and wash off contaminants and dust.[2,3] Much effort has been devoted to try to mimic the self-cleaning property of the lotus leaf,[4,5] although little success has been achieved thus far. However, an alternative approach, which utilizes the photocatalytic[6] and superhydrophilic[7,8] properties of TiO_2, has achieved considerable success. Some TiO_2-based self-cleaning products such as tiles, glass, and plastics have become commercially available.[9,10] One of the advantages of this kind of self-cleaning surface is that TiO_2 can decompose organic contaminants[11] or kill bacteria adhering to the surface[12] under ultraviolet (UV) illumination. Moreover, the superhydrophilic TiO_2 coating favors the fast and complete spreading of water droplets on the surface, which also aids the decontamination process.

TiO_2-based coatings can be applied easily on transparent substrates such as glass and plastics to provide a self-cleaning function. However, the coatings developed thus far always enhance the surface reflection of transparent substrates due to the large refractive index of TiO_2 ($n \approx 2.52$ for anatase; 2.76 for rutile). Reflection at the air−glass interface is about 4% for normal incident light; whereas at the air−TiO_2 interface reflection for normal incident light could be as high as 20%, as described by the simplified Fresnel's equation

$$R = (n_2 - n_1)^2/(n_2 + n_1)^2 \qquad (1)$$

where n_1, equal to 1, is the refractive index of air environment, and n_2 is the refractive index of solid substrates. However, in many applications, including solar cells, light fixtures, greenhouses, etc., self-cleaning coatings with low surface reflection, i.e., high light transmittance, are favored.

Antireflection (AR) coatings are widely used to reduce the surface reflection of optical devices. The principle of AR is interference of the reflected light from the air−coating and coating−substrate interfaces. Thus, the AR coating should exhibit a refractive index between that of the air and the substrate. An ideal homogeneous single-layer AR coating should satisfy the following conditions: the thickness of the coating should be $\lambda/4$, where λ is the wavelength of the incident light; and $n_c = (n_a \times n_s)^{0.5}$, where n_c, n_a, and n_s are

* Corresponding author. E-mail: Fujishima@kast.or.jp. Fax: +81-44-819-2038. Tel: +81-44-819-2020.
† Kanagawa Academy of Science and Technology.
‡ Keio University.

(1) Blossey, R. *Nat. Mater.* **2003**, *2*, 301.
(2) Barthlott, W.; Neinhuis, C. *Planta* **1997**, *202*, 1.
(3) Feng, L.; Li, S.; Li, Y.; Li, H.; Zhang, L.; Zhai, J.; Song, Y.; Liu, B.; Jiang, L.; Zhu, D. *Adv. Mater.* **2002**, *14*, 1857.
(4) Nakajima, A.; Hashimoto, K.; Watanabe, T. *Monatsh. Chem.* **2001**, *132*, 31.
(5) Gu, Z.-Z.; Uetsuka, H.; Takahashi, K.; Nakajima, R.; Onishi, H.; Fujishima, A.; Sato, O. *Angew. Chem.* **2003**, *115*, 922.
(6) Fujishima, A.; Rao, T. N.; Tryk, D. A. *J. Photochem. Photobiol. C: Photochem. Rev.* **2000**, *1*, 1−21.
(7) Wang, R.; Hashimoto, K.; Fujishima, A.; Chikuni, M.; Kojima, E.; Kitamura, A.; Shimohigoshi, M.; Watanabe, T. *Nature* **1997**, *388*, 431−432.
(8) Wang, R.; Hashimoto, K.; Fujishima, A.; Chikuni, M.; Kojima, E.; Kitamura, A.; Shimohigoshi, M.; Watanabe, T. *Adv. Mater.* **1998**, *10*, 135−138.
(9) Fujishima, A.; Hashimoto, K.; Watanabe, T. *TiO_2 Photocatalysis: Fundamentals and Applications*; BKC: Tokyo, 1999.
(10) Mills, A.; Lepre, A.; Elliott, N.; Bhopal, S.; Parkin, I. P.; O'Neil, S. A. *J. Photochem. Photobiol. A. Chem.* **2003**, *160*, 213−224.
(11) Minabe, T.; Tryk, D. A.; Sawunyama, P.; Kikuchi, Y.; Hashimoto, K.; Fujishima, A. *J. Photochem. Photobiol. A: Chem.* **2000**, *137*, 53−62.
(12) Kikuchi, Y.; Sunada, K.; Iyoda, T.; Hashimoto, K.; Fujishima, A. *J. Photochem. Photobiol. A: Chem.* **1997**, *106*, 51.

Scheme 1. Flow Chart for the Preparation of TiO_2-SiO_2 Self-Cleaning Coatings with Antireflection Properties

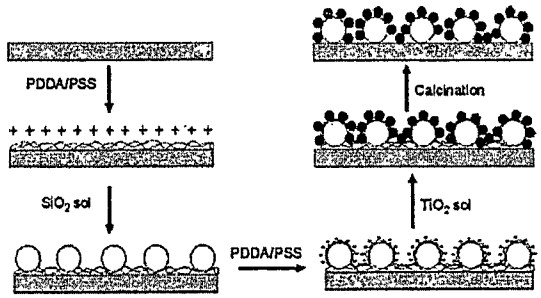

the refractive indices of the coating, air, and substrate, respectively.[13] If n_s is 1.52, as for glass or transparent plastics, n_c must be 1.23 to achieve zero reflection. Since this value is lower than that of any homogeneous dielectric material, AR coatings always adopt 2- or 3-dimensional porous structures to meet the requirement for very low average refractive index.[13–17] Here, we report that a particle coating deposited from submicrometer-sized SiO_2 particles and nanosized TiO_2 particles by stepwise electrostatic deposition showed both self-cleaning and AR properties. Due to the special structure of the coating, the deposited TiO_2 particles did not increase the surface reflection of the glass substrate, but instead improved the AR property of the coating.

Experimental Section

Materials. Poly(diallyldimethylammonium) (PDDA, Aldrich, medium MW and very low MW) and sodium poly(4-styrene sulfonate) (PSS, Aldrich, MW 70 000) were available commercially and were used without further purification at a concentration of 2 mg mL^{-1} in deionized water. PDDA is a linear quaternary ammonium polycation, and PSS is a linear polyanion. Aqueous SiO_2 colloid solution (MP1040, Nissan Kagaku, Japan) was purified by centrifugation and diluted to a concentration of 100 mg mL^{-1} (pH ~9) with deionized water. Aqueous TiO_2 colloid solution (STS-01, pH ~1.5, Ishihara Sankyo, Japan) was diluted to provide concentrations of 1, 10, and 100 mg mL^{-1}. The colloidal SiO_2 particles were negatively charged, while TiO_2 particles were positively charged in the above solutions, since the point of zero charge (PZC) was 2.1 for SiO_2 and 5.5 for TiO_2. Octadodecyldimethylchlorosilane (Gelest) and anhydrous toluene (Aldrich) were used as purchased without further purification. Deionized water with a specific resistance of approximately 18 MΩ cm was used in all experiments.

Preparation of Particle Coatings. The preparation of the TiO_2–SiO_2 coating is summarized in Scheme 1. Glass substrates were cleaned with a concentrated H_2SO_4/H_2O_2 (7:3 v/v) solution and then washed with deionized water. (Caution: the H_2SO_4/H_2O_2 solution is highly dangerous and must be used with great care). The washed substrates were alternatingly dipped in PDDA and PSS solutions for 5 min, with intermediate water washing. Multilayers of (PDDA/PSS)$_4$/PDDA were prepared and used in all experiments. SiO_2 particles were deposited onto the polymer alternative layers by the same procedures, except that a colloidal SiO_2 solution was used. The above procedure is similar to that used by Hattori for the preparation of SiO_2 particle-based AR coatings.[17] The SiO_2 particle coatings were either calcined at 500 °C for 1 h to remove the polymers or were used directly in the subsequent experiments.

In the subsequent step, single layers of SiO_2 particles were covered with low-MW PDDA and PSS alternatingly for two cycles. At this stage, the terminal layer was PSS instead of PDDA. Then, TiO_2 particles were deposited onto the single-layer SiO_2 particles by immersing the substrates into TiO_2 colloid solutions of different concentrations for 5 min followed by extensive washing with deionized water. The as-prepared coatings were calcined at 500 °C for 1 h to remove polymer.

Self-Cleaning Experiment. The calcined TiO_2–SiO_2 particle coatings were modified with a monolayer of octadodecyldimethylchlorosilane (ODS). Typically, the coated glass substrates were preheated at 140 °C for 2 h and then dipped into a 1% solution of ODS in anhydrous toluene. After the coatings were refluxed overnight under N_2, they were removed from the ODS solution and washed with ethanol. The coatings were hydrophobic after treatment. Next, the ODS-modified substrates were placed under black-light lamps, which emit ultraviolet light in the UV-A band. Then, the self-cleaning properties of the TiO_2–SiO_2 coatings were evaluated by measuring the water contact angle at 10 different positions on the films at intervals during irradiation. The intensity of light irradiated on the surface was 1.0 mW cm^{-2} in all experiments, as measured with a Topcon power meter. In control experiments, we also treated SiO_2-particle coatings with ODS and measured the water contact angle on the surface during irradiation.

Other Measurements. Transmission spectra of the particle coatings were measured with a Shimadzu UV3100 spectrophotometer at normal incidence. Surface morphology and cross-sections of the coatings were examined with scanning electron microscopes (SEM, Philips FP6800 and Hitachi S-4500). All of the samples were coated with osmium or platinum with commercial sputtering apparatuses prior to the SEM measurements. The refractive indices of the particle coatings were measured with an ellipsometer (J. A. Woollam, M-2000U) in the wavelength region of 250–1000 nm. The contact angle was measured with a contact angle meter (Kyowa CA-X) in the sessile mode at room temperature and analyzed with commercial FMAS software. In addition to the conventional static contact angle measurements, this software also enabled us to measure the transient contact angle during the spreading of the liquid droplet on the surface. IR reflection spectra for coatings deposited on single-crystal silicon wafers were recorded with a JACSO Irtron IRT-30 infrared microscope.

Results and Discussion

AR Properties. Figure 1 shows the transmission spectra of several particle coatings. The transmittance of the glass substrates was in the 90–92% range for light in the wavelength region of 350–800 nm. Covering both sides of the glass substrate with spherical SiO_2 particles increased the transmittance in the whole spectrum, with the most transmissive wavelength being 530 nm. At this wavelength, the transmittance of the glass substrates coated with SiO_2 particles was as high as 98.33%. Therefore, the SiO_2 particle coating prepared by the electrostatic attraction method acts as an efficient AR coating for glass substrates. The optical thickness of the SiO_2 coating, equal to a quarter of the most transmissive wavelength, was 132.5 nm. This value is close to the average diameter of SiO_2 particles (126 ± 13 nm).

(13) Yoldas, B. E. *Appl. Opt.* **1980**, *19*, 1425–1429.
(14) Minot, M. J. *J. Opt. Soc. Am.* **1976**, *66*, 515–519.
(15) Hiller, J.; Mendelsohn, J. D.; Rubner, M. F. *Nat. Mater.* **2002**, *1*, 59–63.
(16) Walheim, S.; Schäffer, E.; Mlynek, J.; Steiner, U. *Science* **1999**, *283*, 520.
(17) Hattori, H. *Adv. Mater.* **2001**, *13*, 51–54.

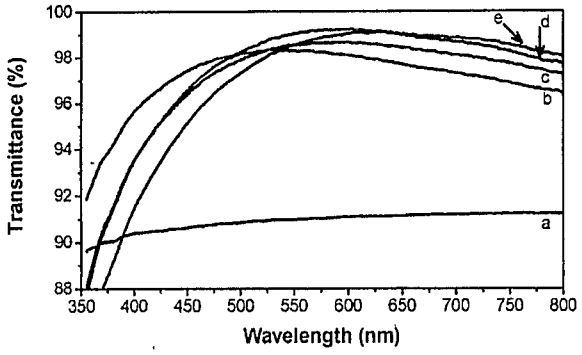

Figure 1. Transmission spectra of several particle coatings on glass substrates at normal incidence: (a) glass substrate; (b) SiO_2 particle coating; and (c) T-1; (d) T-10; and (e) T-100 TiO_2–SiO_2 particle coatings.

The SiO_2 particle coatings were subsequently coated with TiO_2 nanoparticles by the same electrostatic attraction method. The TiO_2 nanoparticles used were from a commercially available colloidal anatase solution, with an average particle size of approximately 30 nm. As shown in Figure 1, additional TiO_2 layers shifted the transmittance band of the SiO_2 particle coatings to longer wavelengths. The maximum transmittance was approximately 590 nm for coatings prepared from 1 mg mL^{-1} TiO_2 (T-1) and 10 mg mL^{-1} TiO_2 (T-10) solution, corresponding to an optical thickness of 147.5 nm; and was approximately 630 nm for a coating prepared from 100 mg mL^{-1} TiO_2 (T-100) solution, corresponding to an optical thickness of 157.5 nm. This shift of transmittance band was reasonable since the deposition of TiO_2 particles increased the average thickness of particle coatings. Although the transmittance in the short-wavelength region (λ < 500 nm) decreased after depositing TiO_2 nanoparticles on SiO_2 particle coatings due to the enhanced scattering of particle layers, the transmittance for the visible light (400–800 nm) was still greater than that of glass substrates for all the TiO_2–SiO_2 particle coatings. Suprisingly, the additional TiO_2 particle layers further improved the maximum transmittance of the glass substrates, though TiO_2 particles exhibited a much larger refractive index than that of the glass substrate. The maximum transmittances were about 98.67% for T-1, 99.22% for T-10, and 99.09% for T-100, respectively. We repeated these experiments several times, and all of the phenomena described above were reproducible.

Figure 2 shows electron micrographs of several AR coatings. The SiO_2 particles were randomly packed on the glass substrate and were deformed from their original spherical shapes due to calcination at 500 °C (Figure 2a). Coating with TiO_2 particles roughened the surfaces of the SiO_2 particles, and the average particle diameter increased to 138 ± 13 nm for T-1, as shown in Figure 2b. The AR coating of T-10 showed a surface morphology similar to that in Figure 2b, except for the slightly larger average particle diameter of 141 ± 12 nm. When 100 mg mL^{-1} TiO_2 solution was used, it was impossible to estimate the particle size, since the SiO_2 particles were overlapped completely by TiO_2 nanoparticles (Figure 2c). These images show that the high TiO_2 concentration favored electrostatic adsorption. This phenomenon is difficult to explain by the principles of electrostatic deposition, since the amount of deposition should be determined by the built-up charge density on the substrate surface instead of the concentration of dipping solution. However, in the electrostatic deposition of colloidal particles, we must take the Coulombic repulsion among the

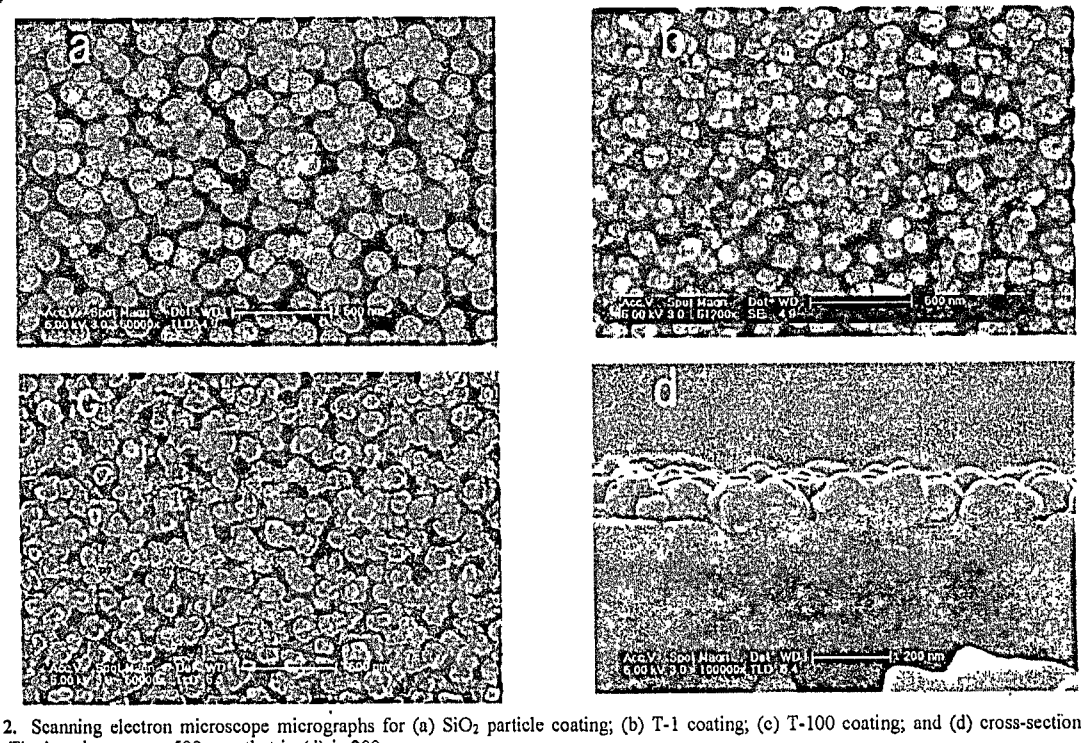

Figure 2. Scanning electron microscope micrographs for (a) SiO_2 particle coating; (b) T-1 coating; (c) T-100 coating; and (d) cross-section of T-100 coating. The bars in a–c are 500 nm; that in (d) is 200 nm.

particles into account, besides the electrostatic attraction among the particles and polymer multilayers. Actually, Lvov et al. have reported the similar concentration-dependent electrostatic deposition of SiO_2 particles multilayers.[18] They have explained this phenomenon by (1) the increased ionic strength at high SiO_2 concentrations, which lowers the Coulombic repulsion among the particles; and (2) the possible aggregation of particles in solution at high SiO_2 concentration.[18] These explanations are reasonable and should also be valid for the concentration-dependent deposition of TiO_2 nanoparticles on SiO_2 particle layers. The concentration effect on the deposition of TiO_2 particles can explain the red-shift of the transmittance band of the T-100 coatings from those of the T-1 and T-10 coatings (Figure 1), since the high coverage of TiO_2 particles and the possible aggregation at high concentration will increase the apparent optical thickness of the TiO_2–SiO_2 particle coatings.

As a characteristic property of electrostatic deposition, almost all of the surface curvature of the submicrometer-sized SiO_2 particles was able to be coated with TiO_2 nanoparticles as shown in the cross-section micrograph (Figure 2d). Such morphology is very important for the self-cleaning properties, as we will discuss below. The refractive indices of the particle coatings at 633 nm, simulated by the Cauchy dispersion model, were 1.16 for the SiO_2 coating, 1.18 for the T-1 coating, 1.21 for the T-10 coating, and 1.25 for the T-100 coating. The gradual increase in the refractive indices of the three TiO_2–SiO_2 coatings is further evidence for the concentration-dependent electrostatic deposition of TiO_2 particles on SiO_2 coatings, since the refractive indices of the particle coatings are related to the volume fractions of SiO_2 particles, TiO_2 particles, and air.[19] The porosity of the SiO_2 particle coating is about 0.685, as calculated from the equation of Yoldas.[13] Such a high porosity suppresses the contribution of the large refractive index of TiO_2 particles, and ensures the TiO_2–SiO_2 particle coatings exhibit low enough refractive indices to induce AR effect. The refractive indices of the TiO_2–SiO_2 coatings are closer than that of the SiO_2 coating to the refractive index (n_c~1.23) of an ideal AR coating for the glass substrate, which can explain the enhanced maximum transmittance of TiO_2–SiO_2 coatings.

Photocatalytic Properties. The TiO_2–SiO_2 particle coatings had a two-component surface, in which both TiO_2 and SiO_2 particles were exposed to the ambient environment. To evaluate the self-cleaning properties of the coatings, the conventional dye adsorption–decomposition method[20] is not valid, since dye molecules such as methylene blue do not adsorb well on the SiO_2 particles. We thus developed another method to study the self-cleaning properties of the TiO_2–SiO_2 particle coatings. In this method, both TiO_2 and SiO_2 particles were first modified with an ODS monolayer on their surfaces. The reactions of ODS molecules with titania and silica have been well studied by Fadeev et al., and the reported grafting densities were approximately 1.5 molecules/nm^2 on TiO_2 and 3 molecules/nm^2 on SiO_2.[21,22] This surface modification made the particle coatings hydrophobic, with contact angles larger than 120°. The hydrophobic alkyl chains of ODS molecules can be decomposed by TiO_2 particles under UV irradiation; the silanol species left on the surface of particles, however, are hydrophilic. Thus, it is possible to evaluate the self-cleaning properties of the particle coatings by monitoring the change of water contact angle on the ODS-modified surface during UV-irradiation. If the ODS molecules on both TiO_2 and SiO_2 particles were photodecomposed, the water contact angle on the coatings would decrease significantly. If the ODS molecules on the SiO_2 particles remained after UV-irradiation, the water contact angle on the coatings should remain large. UV light with a power of 1.0 mW cm^{-2} was used in this experiment; this is less intense than the UV component of sunlight.

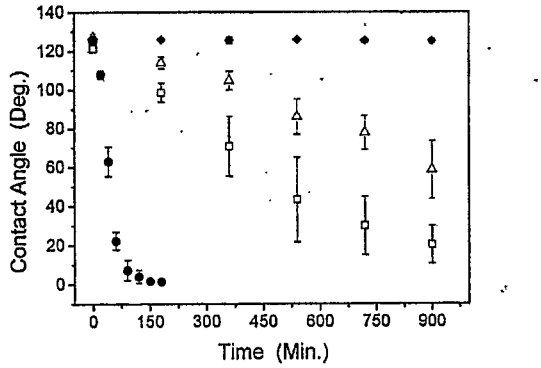

Figure 3. Evolution of water contact angle on several particle coatings modified with octadodecyldimethylsilane monolayers during irradiation with 1.0 mW cm^{-2} ultraviolet light: diamonds, SiO_2 particle coating; triangles, T-1 coating; squares, T-10 coating; and solid circles, T-100 TiO_2–SiO_2 particle coating.

As shown in Figure 3, the water contact angle on the ODS-modified SiO_2 coating changed negligibly during UV-irradiation. In contrast, all of the TiO_2–SiO_2 AR coatings showed significant decreases in water contact angle during irradiation. We found that the rates of contact angle decrease were dependent on the concentrations of the TiO_2 colloid solutions used in the preparation. The fastest decrease of water contact angle was observed for the ODS-modified T-100 coating in three samples. The water contact angle on this coating decreased from 124° to about 0° in 3 h. The ODS-modified T-1 coating showed the slowest decrease of water contact angle in three samples. The water contact angle on this coating only decreased from 125° to 58° in 15 h.

We measured the IR reflection spectra of the ODS-modified T-100 coatings before and after UV-irradiation. There was no IR evidence of alkyl chains on the surface after a 3-h irradiation. Therefore, the alkyl chains of ODS molecules on both TiO_2 and SiO_2 particles were completely

(18) Lvov, Y.; Ariga, K.; Onda, M.; Ichinose, I.; Kunitake, T. *Langmuir* 1997, *13*, 6195–6203.
(19) The refractive indexes (n) of the particle coatings are related to the refractive index and volume fraction of each component by the following equation: $n^2 = (n_{SiO2}^2 V_{SiO2}) + (n_{TiO2}^2 V_{TiO2}) + (n_{air}^2 V_{air})$. We can calculate the volume ratio of TiO_2 to SiO_2 for the three TiO_2–SiO_2 particle coatings from this equation by using the measured refractive indices and the thickness data of the samples. The calculated volume ratios are 1.4% for the T-1 coating, 2.6% for the T-10 coating, and 4.8% for the T-100 coating.
(20) Ohko, Y.; Saitoh, S.; Tatsuma, T.; Fujishima, A. *J. Electrochem. Soc.* 2001, *148*, B24–B25.
(21) Fadeev, A. Y.; McCarthy, T. J. *Langmuir* 1999, *15*, 3759.
(22) Helmy, R.; Fadeev, A. Y. *Langmuir* 2002, *18*, 8924.

Table 1. Water Contact Angles on SiO_2 and TiO_2–SiO_2 Particle Coatings

	SiO_2	T-1	T-100
contact angle	~3°	~1°	~1°

decomposed under UV irradiation. Two principal pathways have been proposed for the TiO_2 photocatalytic oxidation.[6] One is direct photocatalytic oxidation by holes in the valence band of TiO_2. The other is photocatalytic oxidation by the active oxygen species, for example, OH·. The former process occurs on the TiO_2 surface at high reaction rates, whereas the latter process is effective even for organic substances tens of micrometer away from the surface due to the diffusion of the active oxygen species, but it proceeds at slower rates because of the diffusion step.[23] It is clear that the ODS molecules on the SiO_2 particles can be photodecomposed by the latter pathway because of the short distances away from the TiO_2 particles in the composite coatings. The TiO_2 particles first decomposed the ODS molecules on their own surfaces, and subsequently decomposed those on the SiO_2 particles at a slower rate through diffusion of a photogenerated active oxygen species. Therefore, the overall decomposition rates of ODS molecules on the particle coatings were closely related to the coverage of TiO_2 nanoparticles on the SiO_2 single-layer porous structure.

As discussed above, the coverage of TiO_2 nanoparticles on the SiO_2 particles was dependent on the concentration of the colloidal TiO_2 solution. The ODS-modified T-100 coating showed the fastest decrease in water contact angle in which it was used, since it had the highest coverage of TiO_2 particles. It is also possible to increase further the photocatalytic activity of the particle coatings by modifying the deposition conditions.

Surface Wettability. The TiO_2 particle coatings prepared in this manner exhibited excellent wettabilities, as shown in Table 1. Water was able to spread completely on the coatings with contact angles of approximately 1°. This excellent surface wettability is very important for the self-cleaning properties of the coatings.[6] Although the photocatalytic properties of the coatings were dependent on the preparation conditions, the surface wettability was the same for all three samples (T-1, T-10, and T-100). The spreading behavior of water on the as-prepared TiO_2 particle coating showed a negligible difference from that on the UV-treated particle coating (Figure 4). These observations are interesting but unexpected, considering conventional TiO_2 sol–gel coatings and TiO_2 single crystals only showed superhydrophilicity after UV irradiation.[7,8]

One explanation for this unexpected superhydrophilic property is that the large surface roughness of the particle coating improved the surface wettability, as described by the Wenzel model[24]

$$\cos\theta_{\#} = r\cos\theta \qquad (2)$$

Here, the apparent water contact angle $\theta_{\#}$ for a rough surface is lowered from its intrinsic contact angle θ by the roughness factor r, the ratio of the actual to projected area, if θ is smaller than 90°. For example, a flat glass substrate showed a water contact angle of 5°. However, a SiO_2 AR coating showed a better wetting behavior, with a water contact angle of 3° because of the enlarged surface roughness (Table 1). In addition, the TiO_2 nanoparticle layer also plays an important role in the remarkable surface wettability of the coating. In a control experiment, we deposited TiO_2 nanoparticles onto a flat glass substrate by the same method of electrostatic deposition. This surface showed good wettability, with a water contact angle of approximately 1°. It is apparent that the large surface energy of the nanoparticles favors the wetting of water.

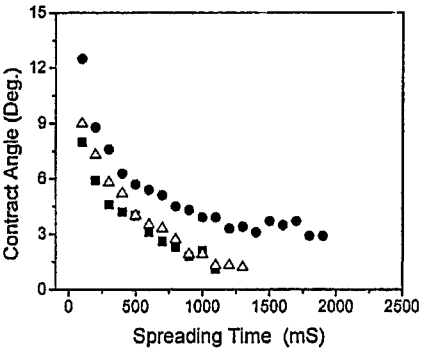

Figure 4. Transient contact angle of 1 μL of water on several particle coatings during spreading: solid squares, as prepared T-100 coating; triangles, T-100 coating after UV-irradiation for 1 h; and circles, as-prepared SiO_2 particle coating.

Conclusions

We have reported here the combination of AR and self-cleaning properties in a core–shell-like TiO_2–SiO_2 particle coating by a simple electrostatic attraction method. A submicrometer-sized SiO_2 particle single layer was used to provide a porous structure with low refractive index, which induces the AR effect. Nanosized TiO_2 particles were coated onto the surface of the SiO_2 layer and were used to provide a self-cleaning, superhydrophilic shell layer. Despite the high refractive index of the TiO_2 nanoparticles, the TiO_2–SiO_2 coatings improved the maximum transmittance of the glass substrates to greater than 99%.

Acknowledgment. This work was supported by a Grant-in Aid for Scientific Research on Priority Areas (417) from the Ministry of Education, Culture, Sports, Science and Technology (MEXT) of the Japanese Government. We thank Dr. D. A. Tryk for carefully reading the manuscript.

Supporting Information Available: SEM pictures (top view and cross-section), and refractive index spectra of the particle coatings, FTIR reflection spectra of ODS-modified TiO_2–SiO_2 particle coating before and after UV-irradiation, and micrograph of water droplets spreading on the TiO_2–SiO_2 particle coating (pdf). This material is available free of charge via the Internet at http://pubs.acs.org.

CM0484201

(23) Tatsuma, T.; Tachibana, S.; Fujishima, A. *J. Phys. Chem. B* **2001**, *105*, 6987–6992.
(24) Wenzel, R. N. *Ind. Eng. Chem.* **1936**, *28*, 988.

附件二

Available online at www.sciencedirect.com
ScienceDirect
ELSEVIER
Journal of Physics and Chemistry of Solids 68 (2007) 2353–2362
JOURNAL OF PHYSICS AND CHEMISTRY OF SOLIDS
www.elsevier.com/locate/jpcs

Modification of multi-walled carbon nanotubes for electric double-layer capacitors: Tube opening and surface functionalization

Chi-Chang Hu[a,*], Jen-Hong Su[a], Ten-Chin Wen[b]

[a]*Department of Chemical Engineering, National Chung Cheng University, Chia-Yi 621, Taiwan*
[b]*Department of Chemical Engineering, National Cheng Kung University, Tainan 701, Taiwan*

Received 15 February 2007; received in revised form 8 April 2007; accepted 9 July 2007

Abstract

Multi-walled carbon nanotubes (MWCNTs) obtained opening the closed ends and using surface functionalization by means of a combination of partial oxidation in air and chemical modifications are characterized systematically in 0.3 M H_2SO_4 between 0 and 1.0 V, and these nanotubes were planned to be used as electrode materials in electric double-layer capacitors (EDLCs). Opening of MWCNTs, clearly observed by means of transmission electron microscopy (TEM), can be easily achieved by the partial oxidation in air through a seven-step temperature program identified by thermogravimetric/differential thermal analyses (TG/DTA). An increase in 175% specific capacitance is obtained for the MWCNTs, partially oxidized in air and chemically modified in $H_2SO_4+HNO_3$. The temperature-programmed desorption (TPD) data showed that evolutions of CO and CO_2 are, respectively, promoted by the application of partial oxidation in air and chemical modification in $H_2SO_4+HNO_3$. The above increase in specific capacitance for modified MWCNTs is attributed to an obvious increase in the BET surface area (double-layer capacitance) and the density of oxygen-containing surface functional groups (pseudocapacitance).

Keywords: C. Thermogravimetric analysis (TGA); D. Electrochemical properties; D. Microstructures

1. Introduction

Electrochemical capacitors are charge storage devices that generally show higher energy density than dielectric capacitors and greater power density and longer cycle life than rechargeable batteries [1–3]. The above unique charge storage/delivery characteristics are attributed to the intrinsic mechanisms of electric energy storage/delivery in electrochemical capacitors: the double-layer and Faradaic redox types. In electric double-layer capacitors (EDLCs), the process of electric charge storage/delivery is due to electrostatic forces between electrode materials and charged species. Hence, no electron transfer across the electrode–electrolyte interface occurs in this typical non-Faradaic process. Since double-layer capacitance is directly proportional to the surface area freely accessible to electrolytes [1,4], carbon in various forms with high-specific surface areas has been widely used as the electrode material for this application [5–8]. For the Faradaic redox process, on the other hand, electron transfer across the electrode–electrolyte interface, with a consequent change in the oxidation state of electroactive materials, occurs in the whole matrix of materials. Thus, electrochemically active materials with several oxidation states/structures and excellent reversibility of charge storage/delivery, such as hydrous transition metal oxides [9–11] and conducting polymers [12–14], have been proposed as promising electrode materials for redox pseudocapacitors.

At present, activated carbons (ACs) are the preferred choice for the electrode materials of EDLCs. Although ACs generally have sufficiently large specific surface areas, their performances in EDLCs are limited in the energy-storage purpose, and they are not suitable for ultrahigh power applications, because most ACs contain high proportions of micropores (diameter<2 nm) [2,3]. The diameter of micropores is so small that the exposed surface

*Corresponding author. Tel.: +886 5 2720411x33411; fax: +886 5 2721206.
E-mail address: chmhcc@ccu.edu.tw (C.-C. Hu).

0022-3697/$ - see front matter © 2007 Elsevier Ltd. All rights reserved.
doi:10.1016/j.jpcs.2007.07.002

is not completely accessible to electrolytes, resulting in the poor utilization. Besides, even under the situation where the micropores are wetted by electrolytes, movement of solvated ions in such small pores may be not fast enough for rapid charge/discharge. Accordingly, a great loss in the specific capacitance is usually found under high-power operation, which is one of the inherent disadvantages of ACs in EDLC application [15].

In contrast with ACs, carbon nanotubes (CNTs) show merits of mesoporous hollow structures, high ratios of electrochemically accessible surface area, excellent electronic conductivity, and good stability. Moreover, pores in CNT electrodes are nano-networked and connected although specific surface areas of CNTs are much lower than that of ACs enriched with micropores [6,8,16]. These unique properties provide possibility of high-power applications of EDLCs [8], even though their specific capacitance is relatively low [17,18]. In order to enhance the specific capacitance of CNTs, several methods have been proposed, such as: (1) chemical activation with KOH or H_2SO_4/HNO_3 to increase the micropores of CNTs [18,19]; (2) oxidation in air [20]; (3) formation of CNT-conducting polymers composites [21–23]; (4) introduction of transition metal oxides into CNTs [24–26]; and (5) electrochemical oxidation of multi-walled carbon nanotubes (MWCNTs) [27]. Unfortunately, applications of these treatments usually decrease the power delivery rate of CNTs, due to variations in the electrochemical reversibility of resultant materials.

Based on the above viewpoints, we propose a simple method to enhance the capacitive performances of MWCNTs, because the cost of single-walled CNTs is very high, and this limits practical interest in it. This method combines partial oxidation in air and chemical modifications in aqueous media to increase the specific surface area freely accessible to electrolytes, to enhance the density of surface functional groups for redox pseudocapacitance, and to maintain the high-power capacity of the resultant MWCNTs. Opening the closed ends and surface functionalization of MWCNTs without significant attack on the sidewall, by proper partial oxidation in air and chemical modification, are the keys to achieve the above requirements. The former contribution is demonstrated through a 7-step temperature-programmed oxidation procedure in air in order to find a suitable temperature (region) for efficiently opening the closed ends of MWCNTs, which can be used to produce MWCNTs with opened ends in a commercial scale. The latter contribution is elucidated by identifying the dependence of mass-based and geometric - specific capacitance on the surface functionalization of MWCNTs. The specific capacitance evaluated by cyclic voltammetry in H_2SO_4 shows that the maximum specific capacitance of modified MWCNTs is about 2.5 times of the raw one. The variations in specific surface area and pore-size distribution are measured by means of nitrogen gas adsorption/desorption isotherms. The microstructures of raw and modified MWCNTs are examined by scanning and transmission electron microscopes (SEM and TEM). The density and distribution of oxygen-containing functional groups within all MWCNTs are qualitatively characterized by temperature-programmed desorption (TPD) analysis.

2. Experimental procedure

MWCNTs with 95% purity, external diameter from 10 to 20 nm, and length from 5 to 15 μm, purchased from Shenzhen Nanotech Port (Nanoport-NTP), served as the basic electrode material in this work (denoted as raw MWCNTs). For the preparation of an MWCNT-coated electrode, 2 mg MWCNTs (with or without modifications) were dispersed in an ethanol solution of 3 cm^3 in an ultrasonic bath. This MWCNT-dispersed solution was dropped onto a $10 \times 10 \times 3\,mm^3$ graphite substrate (Nippon Carbon EG-NPL, N.C.K., Japan) and dried at 80 °C until the ethanol vaporized completely. The average loading of MWCNTs on every electrode is $1.0 \pm 0.05\,mg\,cm^{-2}$. The adhesion of MWCNTs on graphite substrates has been confirmed to be very good. Prior to the coating process, these substrates were abraded with ultrafine SiC paper, degreased with acetone and water, then etched in a 0.1 M HCl solution at room temperature for 10 min, and finally degreased with water in an ultrasonic bath. The exposed geometric area of all pretreated graphite substrates is equal to 1 cm^2 while the other surface areas were insulated with PTFE (polytetrafluorene ethylene) coatings.

Raw MWCNTs, partially oxidized in an oven under an airflow of $250\,cm^3\,min^{-1}$ through a temperature program determined by means of thermogravimetric analysis (Perkin-Elmer Instruments, Diamond TG/DTA), were denoted as MWCNT-1. After this partial oxidation, some of the MWCNT-1 was ultrasonically modified in a mixture of H_2SO_4 (97%) + HNO_3 (65%) with volume ratio 3:1 or an aqueous solution consisting of H_2O_2 (35%), NH_4OH (28%), and H_2O in the volume ratio 1:4:8 for 4 h (the former denoted MWCNT-2 and the latter denoted MWCNT-3). The sonochemically modified MWCNTs were then obtained in a centrifuge and thoroughly washed with pure water several times until pH of the aqueous MWCNTs solution was above 6. Finally, the modified MWCNTs were dried in a vacuum oven overnight (>8 h) at room temperature for electrochemical and textural analyses.

The weight of MWCNTs on each electrode was measured through a microbalance with an accuracy of 10 μg (Sartorius BP 211D, Germany). The specific surface area and pore volume of MWCNTs were determined with an automated adsorption apparatus (Porous Materials, BET-202A) with liquid nitrogen adsorption at −196 °C. The specific surface area and micropore volumes of MWCNTs were calculated on the basis of Brunauer–Emmett–Teller (BET) and Dubinin–Radushkevich (DR) equations [28], respectively. The TPD technique was

employed to analyze the population of oxygen-containing surface functional groups on all kinds of MWCNTs under a helium flow of 30 $cm^3 min^{-1}$ from room temperature to 950 °C at a constant heating rate (10 °C min^{-1}). The morphology of MWCNTs was characterized by field emission SEM (Hitachi S4800-1, Tokyo). The nanostructures of MWCNTs were examined through a transmission electron microscope (TEM, JEOL JEM-2010).

Electrochemical measurements for all MWCNT-coated electrodes were performed by means of an electrochemical analyzer system, CHI 633A (CH Instruments, USA). All experiments were carried out in a three-compartment cell. An Ag/AgCl electrode (Argenthal, 3 M KCl, 0.207 V vs. SHE at 25 °C) was used as the reference and a piece of platinum gauze with an exposed area equal to 4 cm^2 was employed as the counterelectrode. A Luggin capillary, whose tip was set at a distance of 1–2 mm from the surface of the working electrode, was used to minimize errors due to iR drop in the electrolyte.

All solutions used in this work were prepared with 18 MΩ cm water produced by a reagent water system (MILLI-Q SP, Japan), and all reagents not otherwise specified in this work were Merck, GR. The electrolytes used to study the capacitive behavior of various MWCNTs were degassed with purified nitrogen gas before measurements and nitrogen was passed over the solutions during the electrochemical measurements. The solution temperature was maintained at 25 °C by means of a water thermostat (HAAKE DC3 and K20).

3. Results and discussion

3.1. Tube opening, surface functionalization, and characterization of MWCNTs

The dependence of weight loss and heat evolution on the temperature program for the partial oxidation of raw MWCNTs in air, examined by TG/DTA analyses, are shown in Fig. 1. The slight weight loss during the first two steps (i.e., temperature increasing from ca. 30–400 °C at 10 °C min^{-1} and keeping at 400 °C for 30 min) indicates the evaporation of adsorbed H_2O and evolution of CO_2 from certain oxygen-containing functional groups. The minor increase in weight during step 3 (see curve b) is probably due to the oxidation of amorphous carbon to form surface oxides and/or oxidation of metallic catalysts within the CNTs. Actually, raw MWCNTs were slightly damaged in steps 5 and 6 since the weight loss after step 6 is only ca. 7.5%, which is close to the purity of raw MWCNTs used in this work. On the other hand, significant weight loss is clearly found in step 7, indicating the oxidative damage of MWCNTs. This statement is supported by the sharp increase in heat evolution during this step (see curve c), indicating significant oxidation of MWCNTs into CO_2. Accordingly, step 7 is proposed to be oxidative disruption of tips for MWCNTs since the closed ends of CNTs are relatively weak in comparison with their tubular walls [29]. The yield of MWCNTs after this partial oxidation process is 72.6% from curve b.

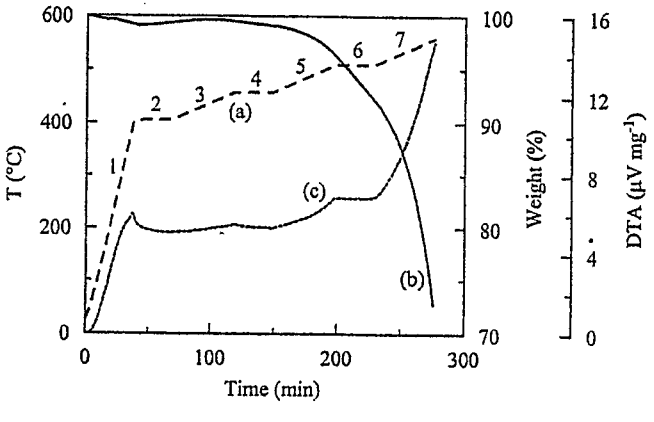

Fig. 1. (a) The temperature program, (b) TGA, and (c) DTA results of raw MWCNTs in a seven-step temperature-programmed oxidation under an airflow of 100 $cm^3 min^{-1}$.

The closed end opening of raw MWCNTs after the partial oxidation can be clearly observed by HRTEM images (see Fig. 2). Raw MWCNTs generally show the closed caps and cylindrical walls, which are uncapped and show rough "convex–concave" walls [30] through the partial oxidation program. These disfigurements enlarge the specific surface area and pore volume of the oxidized MWCNTs (see below).

Based on the above results and discussion, 0.5 g raw MWCNTs were uniformly dispersed onto an alumina crucible (100 × 100 × 20 mm^3) and partially oxidized in an oven under an airflow through the above temperature program. After this partial oxidation program, MWCNTs were rapidly cooled to room temperature. These MWCNTs were denoted as MWCNT-1 and the yield obtained in this relatively large-scale process is 70.1%, which is very close to that determined by means of TG/DTA. Some of MWCNT-1 were subjected to ultrasonic modification in either a concentrated $H_2SO_4 + HNO_3$ mixture or an aqueous solution consisting of H_2O_2, NH_4OH, and H_2O for 4 h to obtain MWCNT-2 and MWCNT-3, respectively.

The closed end opening of raw MWCNTs through the partial oxidation program was confirmed from a comparison of the pore data of all MWCNTs, which were determined from N_2 adsorption/desorption isotherms (see Tables 1 and 2). Note that all modified MWCNTs have a very similar value of BET specific surface area (ca. 200 ± 10 $m^2 g^{-1}$) which is much higher than that of their raw material (ca. 150 $m^2 g^{-1}$). In addition, the pore volume and mean diameter (D_{mean}) of pores for modified MWCNTs are, respectively, larger and smaller than those of raw MWCNTs. These results support the statement that the closed ends of MWCNTs can be selectively opened by the partial oxidation process. Hence, the double-layer capacitance of these modified MWCNTs must be much larger than that of their raw material. Note that the mean pore diameter, D_{mean}, in Table 1 is defined as $4V_{tot}/S_p$ [6]. This parameter is used to estimate the average pore size of

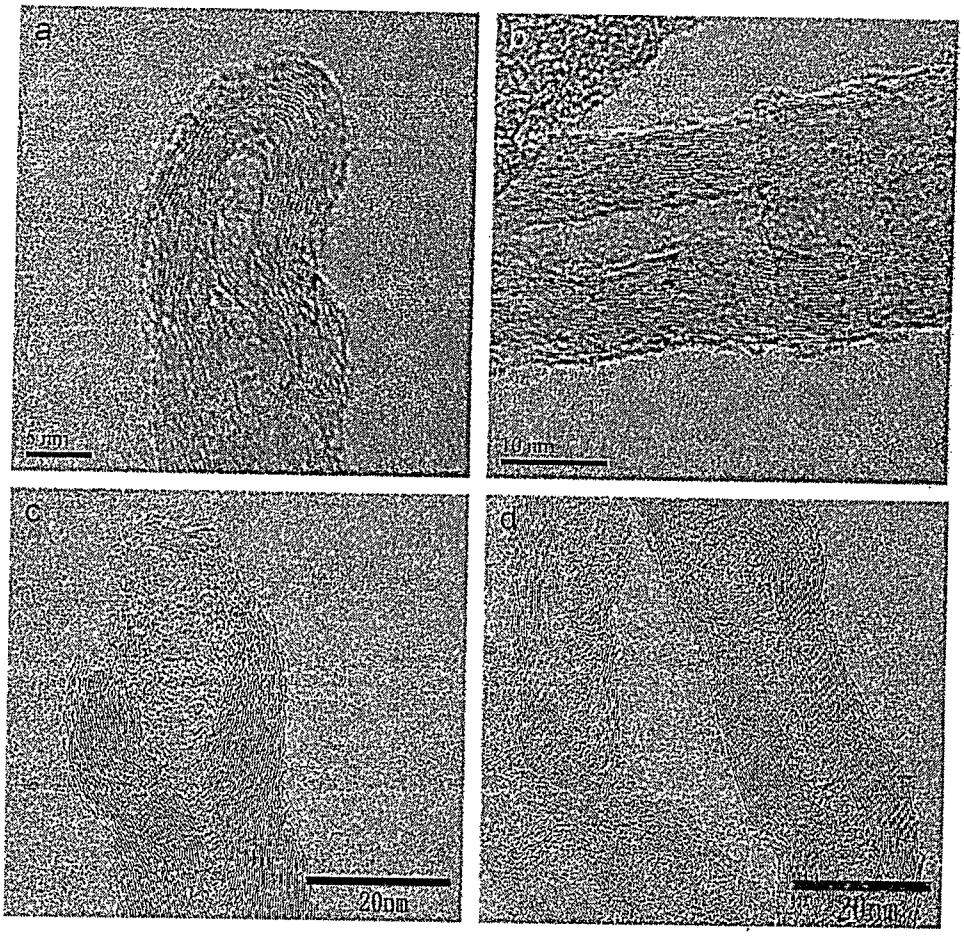

Fig. 2. HR-TEM morphologies of (a,b) raw MWNTs and (c,d) MWNT-1.

Table 1
Pore properties of raw MWCNTs, MWCNT-1, MWCNT-2, and MWCNT-3

CNTs	S_{BET} ($m^2 g^{-1}$)	V_{tot} ($cm^3 g^{-1}$)	V_{mi} ($cm^3 g^{-1}$)	V_{me} ($cm^3 g^{-1}$)	D_{mean} (nm)	C_S($F g^{-1}$)
Raw	148.6	0.79	0	0.79	21.2	12.2
MWNTs-1	208.5	0.84	0	0.84	16.1	30.7
MWNTs-2	209.9	0.95	0	0.95	18.1	33.5
MWNTs-3	194.6	1.01	0	1.01	17.9	27.7

S_{BET}: specific BET surface area; V_{tot}: total volume; V_{mi}: micropore volume; V_{me}: mesopore volume; D_{mean}: mean pore diameter $= 4V_{tot}/S_p$ [6].

Table 2
Pore diameter distributions of raw MWCNTs, MWCNT-1, MWCNT-2, and MWCNT-3

Pore diameters (nm)	Pore size distribution relative to the total pore volume (%)			
	Raw	MWNTs-1	MWNTs-2	MWNTs-3
2.0–5.0	5.5	7.5	9.6	7.1
5.0–10.0	8.0	11.0	10.7	12.3
10.0–15.0	8.5	9.5	8.8	9.1
15.0–20.0	7.7	9.5	10.7	10.5
20.0–30.0	20.0	18.6	23.8	23.1
30.0–40.0	20.2	22.0	21.3	23.0
40.0–50.0	13.8	12.2	8.1	6.9
> 50	16.2	9.5	6.9	7.9

all pores (including pores due to entanglement of MWCNTs). The very similar pore properties of all modified MWCNTs suggest that the chemical modifications in aqueous media do not destroy the sidewalls (main body) of MWCNT-1 while both chemical treatments probably add or change the surface oxygen functional groups dispersed on MWCNT-1. Also note that mesopores predominantly contributed to the pore volumes of all MWCNTs (i.e., 2 < diameter < 50 nm). Hence, most BET surface area should be valid for double-layer charge/discharge [31,32] since the pore volume contributed by micropores (diameter < 2 nm) is negligible.

The partial oxidation and chemical modification do not destroy the sidewalls of MWCNTs significantly. This

statement is supported by the HRTEM morphology of MWCNT-1 (see Fig. 2c and d) and the very similar morphologies and diameter distributions (from 10 to 20 nm) of all MWCNTs (e.g., see SEM photographs in Fig. 3 for raw MWCNTs and MWCNT-2). Note that the sidewall surface of raw MWCNTs is relatively smooth and covered with several amorphous carbon particulates. These carbon particulates are removable by the partial oxidation step although they are not completely removed and certain defects seem to be formed on the sidewall surface of the modified MWCNTs. Hence, a combination of partial oxidation in air and chemical modification is believed to be a potential method in modifying the surface properties and opening the closed ends of MWCNTs, resulting in their higher density of surface oxygen-functional groups (see below). Based on the highly porous microstructures of both MWCNT-coated electrodes shown in Fig. 3 and the metallic conductivity of all MWCNTs used in this work, the 3D mesoporous network structure of MWCNT-coated electrodes is ideal for the EDLC application (see the next section), which favors the penetration of electrolytes and maintains the smooth pathways of electron transport.

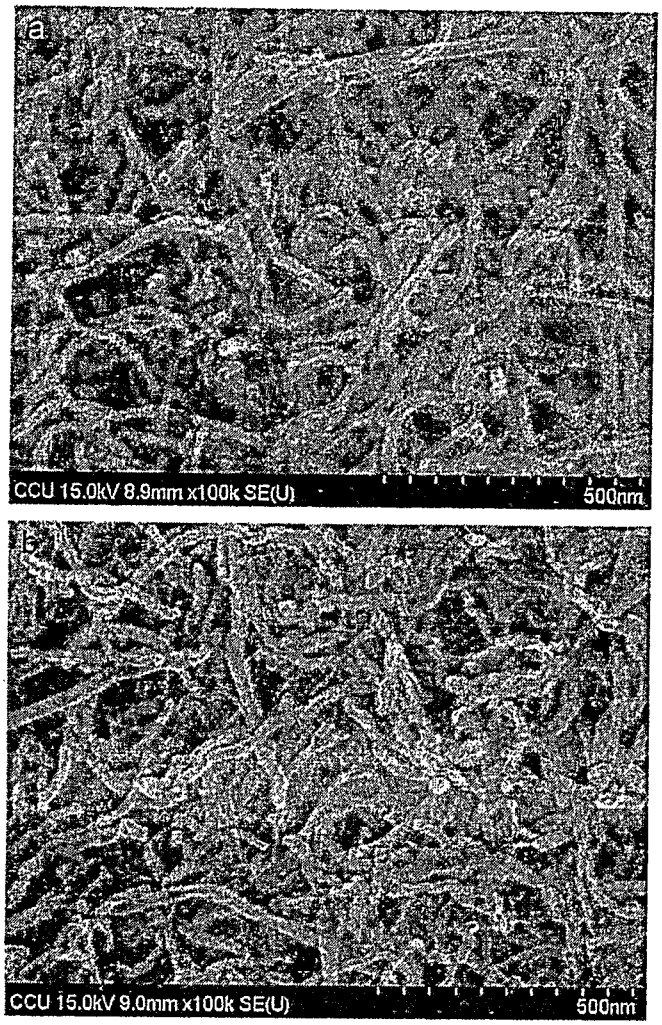

Fig. 3. FE-SEM photographs of (a) raw MWNTs and (b) MWNT-2.

The TPD of CO_2 and CO is often used to identify the population/distribution of oxygen functional groups within pores of carbon-based materials [5–7], which have been classified into several types, such as phenol, carbonyl, carboxyl, quinone, and lactone groups [33]. In addition, these surface functional groups usually exhibit redox and ion exchange abilities which have been found to significantly enhance the specific capacitance of carbon materials [34]. Note that carboxyl and lactone groups will be desorbed as CO_2 when carbons are heated under an inert gas (e.g., He) flow at relatively low temperatures (i.e., $<550\,^{\circ}C$) [5–7,35]. On the other and, hydroxyl, carbonyl, and quinine groups will be desorbed as CO in the relatively high-temperature region ($>500\,^{\circ}C$) [5–7,35]. Accordingly, effects of chemical modifications on the population/distribution of oxygen functional groups can be extensively analyzed from the dependence of CO_2 and CO evolution on the heating temperature. For comparison purposes, raw MWNTs were also subjected to the TPD analysis and typical TPD results of raw MWNTs, MWNT-1, MWNT-2, and MWNT-3 are shown in Fig. 4 as curves 1–4, respectively.

On curve 1, CO_2 evolution corresponding to the decomposition of carboxyl (at 100, 200, and 300 °C) and lactone groups (at 450 °C) is clearly found in the relatively low-temperature region. The desorption of CO species attributable to the quinone groups occurs in the broad temperature region around 700 °C. Both results reveal that raw MWCNTs contain significant amount of oxygen-containing functional groups in various forms (e.g., carboxylic acid, quinine), similar to those observed for carbons in other forms [36–38]. In fact, the presence of oxygen-containing functional groups has been ascribed to the formation of these functional groups either on the adhered amorphous carbon or on the sidewall surface of nanotubes during the purification step (e.g., reflux in nitric acid) [39–41]. The partial oxidation in air raises the

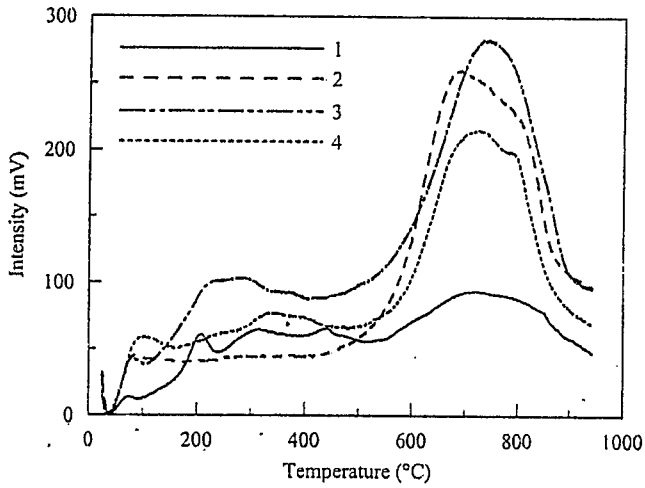

Fig. 4. Evolution profiles of CO_2 and CO by means of the TPD method for (1) raw MWCNTs, (2) MWCNT-1, (3) MWCNT-2, and (4) MWCNT-3.

intensity of CO_2 evolution at temperatures $\leqslant 190\,^{\circ}C$, while the intensity between 190 and 500 °C is slightly reduced, suggesting that removal and formation of carboxyl and lactone groups simultaneously occur during this partial oxidation process (see curve 2). On the other hand, the intensity of CO evolution is sharply increased by the application of this program, indicating the significant formation of hydroxyl, carbonyl, and quinine groups. From a comparison of curves 2–4, the intensities corresponding to CO_2 evolution are nearly featureless for MWCNT-1, which can be increased by the followed chemical modifications. The formation of CO-like surface functional groups is also promoted by the chemical modification in $H_2SO_4+HNO_3$ (see curve 3). Both results reveal the oxidative power of concentrated $H_2SO_4+HNO_3$, favoring the formation of CO_2- and CO-evolving species. On the other hand, the intensities corresponding to CO evolution for MWCNT-3 are obviously reduced by the modification in a mixture consisting of H_2O_2, NH_4OH, and H_2O (see curve 4). This suggests that certain amount of CO-like functional groups formed in the partial oxidation process are further oxidized to form the carboxyl and lactone groups during this modified step. However, this solution cannot significantly attack MWCNT-1 to form the species evolving CO. The above statement is supported by approximately the same areas under curves 2 and 4 in Fig. 4, although chemical modifications of carbon materials should be very complicated.

3.2. Electrochemical characterization of MWCNTs

The excellent reversibility of charge storage and delivery for both raw and modified MWCNTs demonstrates the promising potential in the application of EDLCs (see Fig. 5). The rectangular and symmetric i–E responses on both positive and negative sweeps of curve 1 reveal the ideal capacitive performance of raw MWCNTs. The two pairs of

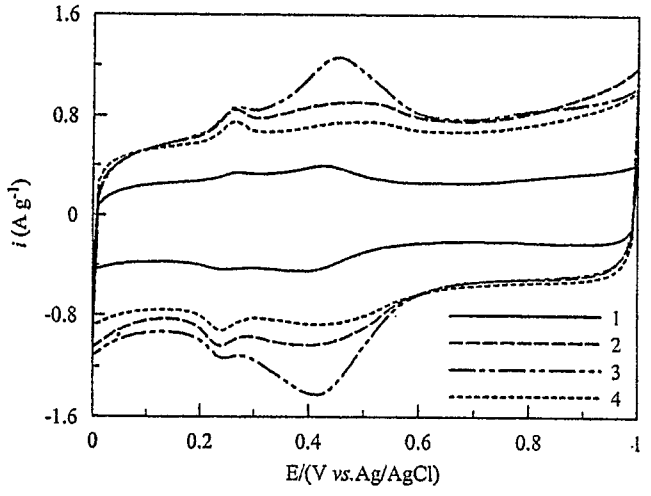

Fig. 5. Cyclic voltammograms of (1) raw MWCNTs; (2) MWCNT-1; (3) MWCNT-2; and (4) MWCNTs-3. CV curves were measured at $25\,mV\,s^{-1}$ in 0.3 M H_2SO_4.

unclear redox peaks centered at around 0.3 and 0.45 V are attributable to the redox transitions of oxygen-containing functional groups evidenced in the TPD study (see Fig. 4). Unfortunately, the specific capacitance (C_S) of raw MWCNTs estimated from this CV curve is only about $12.2\,F\,g^{-1}$ (i.e., $8.2\,\mu F\,cm^{-2}$). Note that the basal plane of graphite has been found to show extremely low geometric specific capacitance (e.g., $<1\,\mu F\,cm^{-2}$) [42]; meanwhile the basal plane of most tubular sidewalls is parallel to the axial direction of MWCNTs (see HRTEM images in Fig. 2). The low specific capacitance of raw MWCNTs is thus reasonably attributed to their graphite nature with the extensive exposure of the basal plane to electrolytes, although the tubular sidewalls are covered with certain amount of amorphous carbons.

The partial oxidation in air is an effective route promoting the capacitive current densities of MWCNTs in the whole potential region of investigation. A net increase of 151.6% in specific capacitance (i.e., from 12.2 to $30.7\,F\,g^{-1}$) is obtained after this application. Moreover, from a comparison of curves 1 and 2 in Fig. 5, there is no sensible increase in iR drop when the sweep direction of CV is changed. This phenomenon indicates no sensible variation in electronic conductivity of MWCNTs after the application of partial oxidation in air. The above increase in specific capacitance is reasonably attributed to a combined effect of the higher BET surface area and the much higher density of oxygen-containing functional groups for MWCNT-1. The former effect should provide ca. 40% increase in C_S since the ratio of BET specific surface area between MWCNT-1 and raw MWCNTs is about 1.4. The extra increase in C_S is ascribed to the pseudocapacitance coming from the redox reactions of oxygen functional groups which have been identified in the TPD study (see Fig. 4). This statement is also supported by the very obvious increase in the geometric specific capacitance from 8.2 to $14.7\,\mu F\,cm^{-2}$. Actually, some articles found that specific capacitance of carbon materials can be enhanced by introducing various surface functional groups through thermal, chemical, or electrochemical routes [5–7,35,43,44]. Certain electroactive groups, such as quinone, hydroxyl, and carbonyl groups, can provide the redox transitions as follow:

$$O=Ph=O+2H^{+}+2e\leftrightarrow HO-Ph-OH \quad (1)$$

$$R=O+H^{+}+e\leftrightarrow R-OH \quad (2)$$

where Ph and R indicate the phenyl and aliphatic groups, respectively. The other functional groups, such as anhydrides and carboxyl groups, are ionic exchangeable or attractable to solvated ions [42,45,46]. Therefore, the number of ions involved in building the electric double layer should be increased (i.e., increase in charge density). Moreover, a higher density of oxygen functional groups was reported to improve the wettability of the carbon surface in aqueous electrolytes, probably further increasing

the utilization of specific surface area for double-layer capacitance [46].

Chemical modifications in oxidative aqueous media do not guarantee further promotion in the specific capacitance of MWCNT-1. The modification in a mixture of $H_2SO_4+HNO_3$ does enhance the specific capacitance ($33.5\,F\,g^{-1}$ for MWCNT-2) while an opposite result is found for MWCNT-3 ($27.7\,F\,g^{-1}$). The modification in $H_2SO_4+HNO_3$ causes an increase in current densities for the redox couple between 0.3 and 0.6 V, probably corresponding to the active surface groups such as C–OH, C = O, and COOH [31,33,42,46,47]. The relatively lower capacitance currents of MWCNT-3 are attributable to the significant reduction in the CO-like functional groups (see Fig. 4), since variations in BET specific surface area, pore volume, and mean pore diameter among all modified MWCNTs are minor.

In order to clarify the influences of the density of surface functional groups on the specific capacitance, a new parameter—degree of functionalization—is introduced here. The total active area of surface functional groups corresponding to CO_2 evolution, A_{SF1}, is defined as the area under the TPD curves at temperature $<525\,^{\circ}C$; meanwhile those corresponding to CO evolution is the area under the TPD curves at temperature $\geq 525\,^{\circ}C$ (denoted as A_{SF2}) to indicate the relative total amount of surface functional groups. Accordingly, the degree of functionalization is defined as the ratio between the active area of functional groups and the BET surface area. These data and F_{Dt} (the sum of F_{D1} and F_{D2}) are shown in Table 3. From a comparison of the functionalization degree and C_S data, several features need to be described. First, F_{D1} and F_{D2} are, respectively, decreased and increased by the closed-end opening step (partial oxidation in air). The decrease in F_{D1} is reasonably attributed to the significant removal of carboxyl and lactone groups in this partial oxidation process although they should be continuously transformed from the CO-like groups during the closed-end opening process. The increase in F_{D2} reveals the effective accumulation of CO-like functional groups through the partial oxidation step. Hence, the obvious increase in geometric specific capacitance from 8.2 to $14.7\,\mu F\,cm^{-2}$ is reasonably due to the contribution of redox pseudocapacitance from the high density of CO-like functional groups of MWCNT-1, since the surface area effect has been normalized. Second, the modification in $H_2SO_4+HNO_3$ further promotes the degree of functionalization (see F_{D1}, F_{D2} and F_{Dt}), causing a further increase in the geometric-specific capacitance from 14.7 to $16.0\,\mu F\,cm^{-2}$. Third, a slight decrease in the geometric specific capacitance from 14.7 to $14.2\,\mu F\,cm^{-2}$ is obtained when MWCNT-1 has been chemically modified with $H_2O_2+NH_4OH$, due to a compromise between F_{D1} and F_{D2}. The above variations in the geometric specific capacitance are completely consistent with F_{D1}, F_{D2} and F_{Dt} data, indicating the fact that the geometric specific capacitance is predictable by the degree of functionalization.

The charge–discharge reversibility of electric double layer is generally good if the pore size of electrode materials with good electronic conductivity is large enough for the movement of solvated ions. On the other hand, the electrochemical reversibility of Faradaic redox transitions for oxygen-containing functional groups is also very important in this work since all MWCNTs exhibit significant amount of surface functional groups and their contribution to specific capacitance is as important as that of the electric double layer. This requirement can be qualitatively examined by varying the upper potential limit of CV in the potential region of investigation (see Fig. 6). From this figure, the i–E curves on the positive sweeps completely follow the same trace for all MWCNTs, indicating that the repeated applications of CV in the potential region of investigation insignificantly influence the distribution of surface functional groups. Moreover, the symmetric i–E responses for all CV curves in Fig. 6 reveal that both double-layer charge/discharge and redox transitions of surface functional groups are highly reversible. This good performance should result from the mesoporous nature of MWCNTs with acceptable electronic conductivities.

The power property of all MWCNTs was also examined in this work to demonstrate their promising applicability, which can be identified from their voltammetric responses at different scan rates (e.g., see Fig. 7a for MWCNT-2). From Fig. 7a, no change in shape without any sensible increase in iR drop is clearly found, although the highest scan rate of CV is 6.7 times of the lowest one. This result reveals the excellent reversibility of the charge storage/delivery process for MWCNT-2, although Faradaic currents are significant in the whole potential region of investigation. The quasi-linear dependence of voltammetric currents for all MWCNTs at 0.45 V shown in Fig. 7b further supports the above statement, which demonstrates

Table 3
Data of the functionalization degree of raw MWCNTs, MWCNT-1, MWCNT-2, and MWCNT-3

CNTs	A_{SF1} (mV)	A_{SF2} (mV)	F_{D1} ($mV\,m^{-2}$)	F_{D2} ($mV\,m^{-2}$)	F_{Dt} ($mV\,m^{-2}$)
Raw	79,992	122,739	538.3	826.0	1364.3
MWNTs-1	76,589	320,263	367.3	1536.0	1903.3
MWNTs-2	140,917	341,586	671.4	1627.4	2298.8
MWNTs-3	108,215	256,886	556.1	1320.1	1876.2

$F_{Dt} = F_{D1} + F_{D2}$.

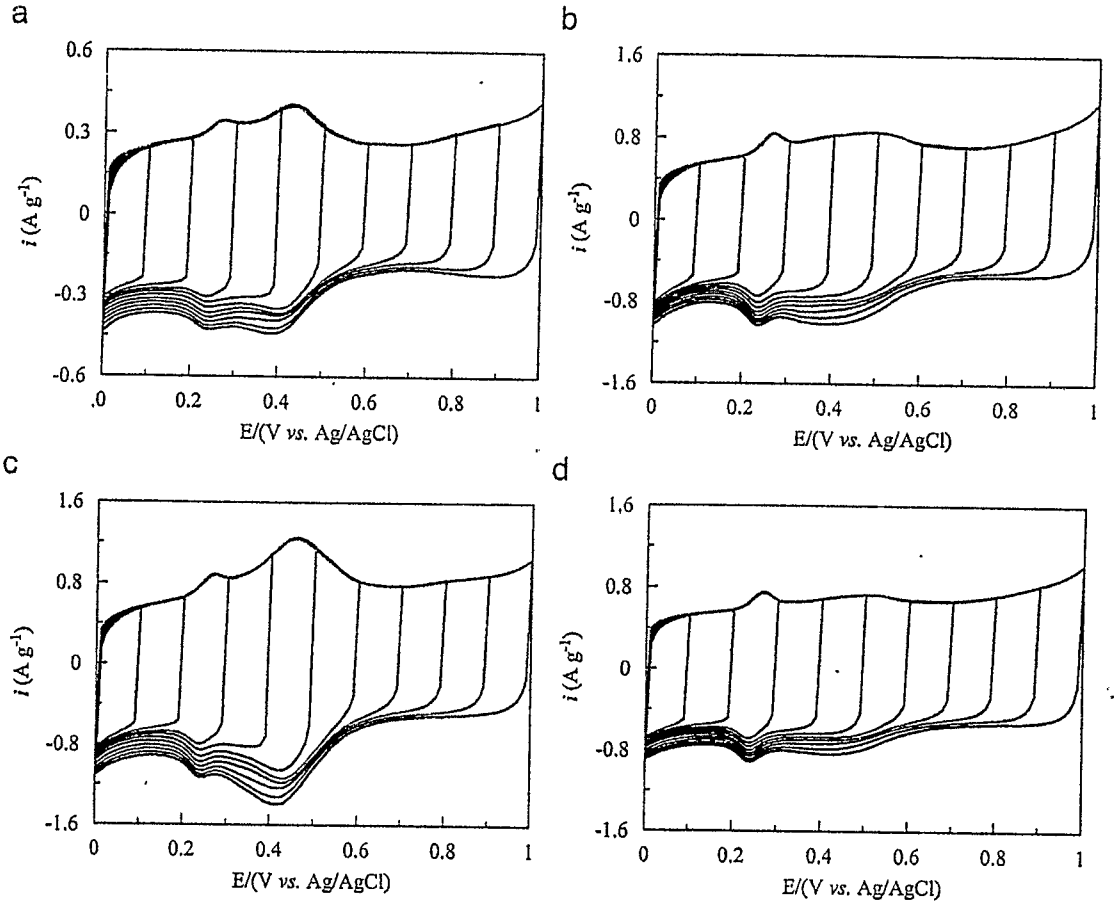

Fig. 6. Cyclic voltammograms of (a) raw MWCNTs, (b) MWCNT-1, (c) MWCNT-2, and (d) MWCNT-3 with varying the upper potential limits of CV. CV curves were measured at 25 mV s^{-1} in 0.3 M H_2SO_4.

the high power property of all MWCNTs studied in this work. The excellent power performance of all modified MWCNTs should result from the insignificant variation in electronic conductivity of MWCNTs after the application of partial oxidation in air and chemical modification. This fact further supports the statement that properly partial oxidation in air and chemical modification in $H_2SO_4+HNO_3$ do not damage the sidewall of MWCNTs significantly, which is the key to increase the specific surface area freely accessible to electrolytes, to introduce surface functional groups for redox pseudocapacitance, and to maintain the high-power capacity of the resultant MWCNTs. Moreover, the quasi-linear dependence of voltammetric currents on the scan rate of CV also reveals that the Faradaic redox reactions only occur at/near the interface of MWCNTs (i.e., similar to a thin-film, reversible adosprtion/desorption process) [42]. This is one of the intrinsic requirements for the electrode materials exhibiting pseudocapacitive responses [1].

4. Conclusions

Partial oxidation in air is a powerful tool in opening the closed ends and enhancing the density of oxygen-containing functional groups of MWCNTs, identified by means of BET and TPD analyses, respectively. This method not only increases the specific surface area of mesopores for the double-layer capacitance, but also enhances the contribution of pseudocapacitance coming from the interfacial redox reactions. The chemical modification of MWCNT-1 in a mixture of $H_2SO_4+HNO_3$ further increases the specific capacitance, but an opposite result is obtained when a solution consisting of H_2O_2 (35%), NH_4OH (28%), and H_2O is employed, due to the decrease in the functionalization degree. An increase in 175% specific capacitance is obtained for MWCNT-2 due to a combination of partial oxidation in air and chemical modification in $H_2SO_4+HNO_3$. All MWCNTs showing excellent capacitive performances in the sulfuric acid solution indicate insignificant damage on the tubular sidewalls during the partial oxidation in air and chemical modifications. Accordingly, a combination of partial oxidation in air through the 7-step program and chemical modification in $H_2SO_4+HNO_3$ is a promising method in promoting the capacitive performances of MWCNTs by increasing the specific surface area freely accessible to electrolytes, enhancing the density of surface functional groups for redox pseudocapacitance, and maintaining the high-power capacity of resultant MWCNTs.

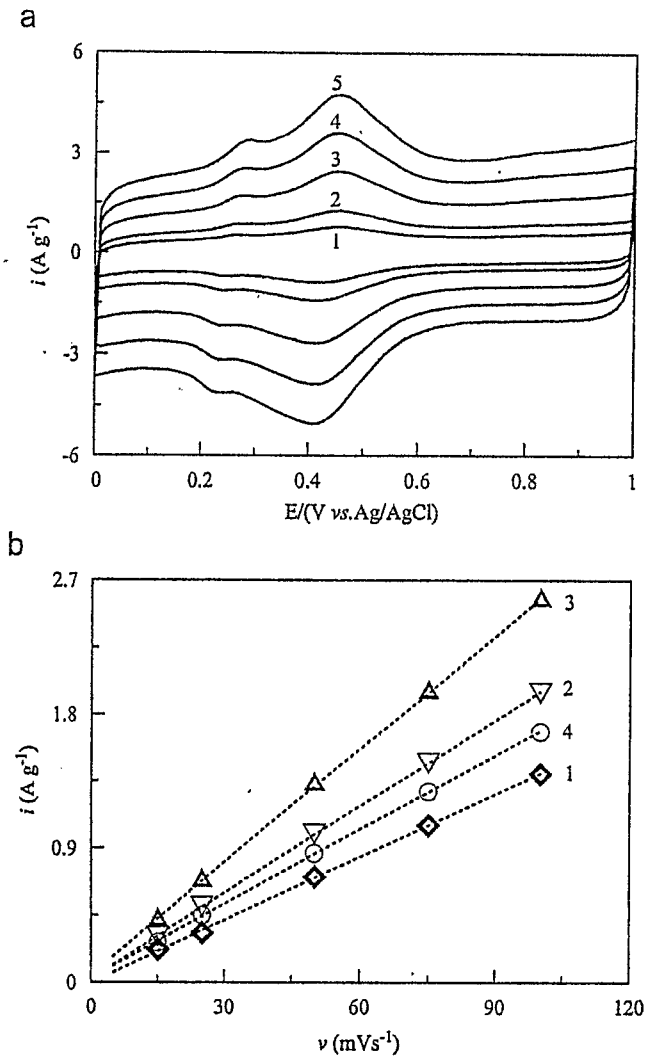

Fig. 7. (a) Cyclic voltammograms of MWCNT-2 measured at (1) 15, (2) 25 (3) 50, (4) 75, and (5) 100 mV s^{-1}; and (b) dependence of the capacitance current density on the scan rate of CV at 0.45 V on the positive sweeps for (1) raw MWNTs, (2) MWCNT-1, (3) MWCNT-2, and (4) MWCNT-3. CV curves were measured in 0.3 M H_2SO_4.

Acknowledgments

Financial support for this work, provided by the National Science Council of the Republic of China under Contract no. NSC 94-2221-E-194-067, is acknowledged. The authors appreciate the reviewer's suggestion on the viewpoint of the functionalization degree of modified MWCNTs.

References

[1] B.E. Conway, Electrochemical Supercapacitors, Kluwer-Plenum Pub. Co, New York, 1999, p. 29.
[2] A. Burke, J. Power Sources 91 (2000) 37.
[3] R. Kotz, M. Carlen, Electrochim. Acta 45 (2000) 2483.
[4] A.J. Bard, L.R. Faulkner, Electrochemical Methods, Fundamentals and Applications, Wiley, Singapore, 1980.
[5] C.-C. Wang, C.-C. Hu, Carbon 43 (2005) 1926.
[6] F.-C. Wu, R.-L. Tseng, C.-C. Hu, C.-C. Wang, J. Power Sources 159 (2006) 1532.
[7] P.-Z. Cheng, H. Teng, Carbon 41 (2003) 2057.
[8] C. Niu, E.K. Sichel, R. Hoch, D. Moy, H. Tennent, Appl. Phys. Lett. 70 (1997) 1480.
[9] C.-C. Hu, C.-Y. Chen, Electrochem. Solid State Lett. 5 (2002) A43.
[10] C.-C. Hu, T.-W. Tsou, Electrochem. Commun. 4 (2002) 105.
[11] C.-C. Hu, K.-H. Chang, M.-C. Lin, Y.-T. Wu, Nano Lett. 6 (2006) 2690.
[12] C.-C. Hu, W.-Y. Li, J.-Y. Lin, J. Power Sources 137 (2004) 152.
[13] K.R. Prasad, N. Munichandraiah, J. Electrochem. Soc. 149 (2002) A1393.
[14] C.-C. Hu, X.-X. Lin, J. Electrochem. Soc. 149 (2002) A1049.
[15] S. Yoon, J. Lee, T. Hyeon, S.M. Oh, J. Electrochem. Soc. 147 (2000) 2507.
[16] B. Zhang, J. Liang, C.L. Xu, B.Q. Wei, D.B. Ruan, D.H. Wu, Mater. Lett. 51 (2001) 539.
[17] E. Frackowiak, K. Jurewicz, S. Delpeux, F. Beguin, J. Power Sources 97–98 (2001) 822.
[18] E. Frackowiak, S. Delpeux, K. Jurewicz, K. Szostak, D. Cazorla-Amoro, F. Beguin, Chem. Phys. Lett. 361 (2002) 35.
[19] C.S. Li, D.Z. Wang, T.X. Liang, X.F. Wang, J. Liang, Mater. Lett. 58 (2004) 3774.
[20] C. Li, D. Wang, T. Liang, X. Wang, J. Wu, X. Hu, J. Liang, Powder Technol 142 (2004) 175.
[21] M. Hughes, M.S.P. Shaffer, A.C. Renouf, C. Singh, G.Z. Chen, D.J. Fray, A.H. Windle, Adv. Mater. 14 (2002) 382.
[22] M. Hughes, G.Z. Chen, M.S.P. Shaffer, D.J. Fray, A.H. Windle, Chem. Mater. 14 (2002) 1610.
[23] Y.K. Zhou, B.L. He, W.J. Zhou, J. Huang, X.H. Li, B. Wu, H.L. Li, Electrochim. Acta 49 (2004) 257.
[24] Y.K. Zhou, B.L. He, F.B. Zhang, H.L. Li, J. Solid State Electrochem. 8 (2004) 482.
[25] X. Qin, S. Durbach, G.T. Wu, Carbon 42 (2004) 451.
[26] J.H. Park, J.M. Ko, O.O. Park, J. Electrochem. Soc. 150 (2003) A864.
[27] J.-S. Ye, X. Liu, H.F. Cui, W.-D. Zhang, F.-S. Sheu, T.M. Lim, Electrochem. Commun 7 (2005) 249.
[28] S. Lowell, J.E. Shields, Powder surface area and porosity, Third ed, Chapman & Hall, New York, 1991.
[29] J.M. Skowronski, P. Scharff, N. Pfander, S. Cui, Adv. Mater. 15 (2003) 55.
[30] P.M. Ajayan, T.W. Ebbesen, T. Lchihashi, S. Iijima, K. Tanigaki, H. Hiura, Nature 362 (1993) 522.
[31] E. Frackowiak, Carbon 39 (2001) 937.
[32] S. Sarangapani, J. Electrochem. Soc. 143 (1996) 3791.
[33] K. Kinoshita, Carbon: Electrochemical and Physicochemical Properties, Wiley, New York, 1988.
[34] H.A. Andreas, B.E. Conway, Electrochim. Acta 51 (2006) 6510.
[35] C.-C. Hu, C.-C. Wang, F.-C. Wu, R.-L. Tseng, Electrochim. Acta 52 (2007) 2498.
[36] K. Kinoshita, J.A.S. Bett, Carbon 11 (1973) 403.
[37] R.L. McCreery, in: A.J. Bard (Ed.), Electroanalytical Chemistry, Marcel Dekker, New York, vol. 17, 1990, p. 221.
[38] G. Che, B.B. Lakshmi, E.R. Fisher, C.R. Martin, Nature 393 (1999) 346.
[39] H. Ago, T. Kugler, F. Cacialli, W.R. Salaneck, M.S.P. Shaffer, A.H. Windle, R.H. Friend, J. Phys. Chem. B 103 (1999) 8116.
[40] J. Liu, A.G. Rinzler, H. Dai, J.H. Hafner, R. Kelley Bradley, P.J. Boul, A. Lu, T. Iverson, K. Shelimov, C.B. Huffman, F. Rodriguez-Macias, Y. Shon, T. Randall Lee, D.T. Colbert, R.E. Smalley, Science 280 (1998) 1253.
[41] A.G. Rinzler, J. Liu, H. Dai, P. Nikolaev, C.B. Huffman, F.J. Rodriguesmacias, P.J. Boul, A.H. Lu, D. Heymann, D.T.

Colbert, R.S. Lee, J.E. Fisher, A.M. Rao, P.C. Eklund, R.E. Smalley, Appl. Phys. A 67 (1998) 29.
[42] P.T. Kissinger, W.R. Heineman (Eds.) Laboratory Techniques in Electroanalytical Chemistry, second ed., Marcel Dekker, New York, 1999.
[43] R.Z. Ma, J. Liang, B.Q. Wei, B. Zhang, C.L. Xu, D.H. Wu, J. Power Sources 84 (1999) 126.
[44] T. Momma, X. Liu, T. Osaka, Y. Ushio, Y. Sawada, J. Power Sources 60 (1996) 249.
[45] J.L. Figueiredo, M.F.R. Pereira, M.M.A. Freitas, J.J.M. Orfao, Carbon 37 (1999) 1379.
[46] C.T. Hsieh, H. Teng, Carbon 40 (2002) 667.
[47] J.H. Jang, S. Han, T. Hyeon, S.M. Oh, J. Power Sources 123 (2003) 79.